Received: 20 February 2021 | Revised: 21 April 2021 | Accepted: 10 May 2021

DOI: 10.1002/kin.21504

RESEARCH ARTICLE

Potentialities of mass spectrometry on activation energy and secondary reactions determination of calcium oxalate thermal decomposition

Renzo Campostrini[1] | **Maurizio Grigiante**[2] | **Marco Brighenti**[2]

[1] Department of Industrial Engineering, University of Trento, Trento, Italy

[2] Department of Civil and Environmental Engineering, University of Trento, Trento, Italy

Correspondence
M. Grigiante, Department of Civil and Environmental Engineering, University of Trento, Via Mesiano 77, 38123, Trento, Italy
Email: maurizio.grigiante@unitn.it

Abstract

This work investigates the potentialities of the thermal analysis (TA) coupled with the mass spectrometry (MS) technique by studying the thermal decomposition of calcium oxalate monohydrate ($CaC_2O_4 \cdot H_2O$). The aim of this work is twofold: to demonstrate, at first, the efficacy of coupling the thermal gravimetric (TG)-MS experimental approach to check the presence of intermediate reactions beyond the conventional three-step decomposition: dehydration, decarbonylation, and decarbonation; second, to test the reliability of different modeling approaches in determining the activation energy (E) including, as innovative alternative, the use of the MS signals. The TA is carried out at selected constant heating rates by recording both the thermal gravimetric analysis, differential thermal analysis) profiles, and, simultaneously from the MS data, the signals of the total ion current and the ion currents selected to monitor the release of the H_2O, CO, and CO_2 species. These experimental results are effective in determining the E through different modeling approaches based on the maximum reaction rate method and isoconversional procedures including both TG and MS signals. Coupling the TA-MS technique has allowed us to check the concurrent presence of the dismutation reaction of carbon monoxide, occurring during the decarbonylation event, and to determine the corresponding E value (E = 169.7 kJ/mol). These results present a surprising correlation between the global enthalpy of the two reactions involved in this second step and their activation energy values. On the whole, the results satisfy the conventional constraints usually adopted to test the reliability of the E results and are consistent with the majority of the datasets published in the literature on this subject.

KEYWORDS
activation energy, calcium oxalate monohydrate, kinetics, mass spectrometry, thermal analysis

1 | INTRODUCTION

Studies on reactions involving solid materials represent a difficult task due to the great variety of factors having different impacts on solid-state reconstruction, diffusion of reaction products and reagents, materials properties, and physical state of the evolving solid-state surface. The experimental techniques involving thermal analysis (TA), including thermogravimetric analysis (TGA), differential thermal analysis (DTA), represent a universal and effective approach for investigating the kinetics of the thermal degradation of solids. Nevertheless, isothermal TGA measurements cannot rigorously be carried out due to the unavoidable presence of finite nonisothermal heat-up time associated with this constraint. At higher temperatures, before reaching the isothermal regime, significant degradations can be observed while, at lower temperatures, a complete conversion can be achieved only by accepting a long reaction time. In addition, at slow heating rates, the weight loss during heat-up time can affect significantly the results of kinetics elaboration.[1,2] Therefore, at an isothermal regime, the nonzero extent of conversion appears particularly critical and the investigations have to be carried out carefully. In constant heating rate analysis, these problems can be avoided by starting at a temperature reasonably below that at which the thermal decomposition starts.[3] The authors are aware that in kinetics it is a good practice to propose a combination of nonisothermal and isothermal analysis. Nevertheless, considering the focus of this work, TA has been limited to a constant heating rate in view of proposing an extended elaboration on further planned investigations.

Under the nonisothermal TGA constraint, quantitative methods can be used to determine kinetic parameters from the TGA curves of which the achievement of the activation energy (E) and the preexponential factor (A) represents the main pursued task. Numerous approaches, including the model-fitting method,[4,5] model-free method,[6,7] and distributed activation energy model method[8,9] have been applied to various kinetic studies.

Coupling the TA with the gas analysis evolving during thermal degradation provides relevant advantages since mass changes can be correlated with the identity of a gaseous volatile compound released during a specific thermal event.[10–12] Among these techniques, TGA coupled with mass spectrometry (TG-MS) can achieve real-time and sensitive detection of evolved gases[13–17] including quantitative information regarding gas product compositions[13,14] as a result of integration elaboration of the evolution profiles for all the detected species. Thus, TG-MS has revealed a precise and sensitive method to investigate the release patterns and identities of volatile components evolving from a multitude of thermal degradation processes as recently proved for coal,[13,15,18] biomass,[17] municipal solid waste,[9] and other materials.[18–21] The TG-MS techniques have been utilized in some of the cited works to detail specific thermal trends: Han et al.[15] discovered that the most prominent peaks of gaseous products evolving during thermal decomposition of lignite samples range from 400 to 700°C; Wang et al.[16] reported the characteristics of gas production by hydrocarbons (HCs) and nonhydrocarbons (nonHCs) during coal pyrolysis and determined its late gas generation potential through TG-MS. To the knowledge of the authors, the use of the TG-MS technique to calculate the kinetic parameters of the solid decomposition is not usually performed since it is mainly utilized to analyze the thermal decomposition data pertaining to the evolved gas phase. Only in a limited number of cases, it is applied to investigate the kinetic parameters of the gaseous species as done by Seo et al.[11] and Nelson et al.[22] for volatiles compounds evolving during coal pyrolysis using single and parallel models.

This work is determined to enhance the potentialities of the TG-MS technique by investigating, as a case test, the thermal decomposition of the calcium oxalate monohydrate ($CaC_2O_4 \cdot H_2O$) and, specifically, it aims to

1. exploit the MS signals to set up an alternative procedure to calculate the E for each single reactions involved in the thermal decomposition of the selected solid besides the apparent E related to the whole event;
2. to make evident the fundamental role of the MS analysis in providing a more correct interpretation of the chemical events occurring during the thermal decomposition of the solids that cannot be completely described by limiting the elaborations only to the signals coming out from the TA.

Regarding the selected compound, two calcium oxalate hydrate forms, referred to as whewellite and weddellite, are the most common. The whewellite, also known as calcium oxalate monohydrate (COM) and here utilized, is the most thermodynamically stable phase. Weddellite, known as calcium oxalate dihydrate (COD), is the metastable form at room temperature while the third hydrate form, indicated as calcium oxalate trihydrate (COT), is rarely observed due to its thermodynamic instability. In addition to their multiple industrial usage, these minerals are heavily studied since calcium oxalate makes up approximately 70% of kidney stones whose formation causes dietary, environmental, genetic diseases,[23] and urolithiasis, the urinary stone disease that affects ~10% of the world's population per generation.[24] Besides these reasons, which make the COM a fully investigated compound,[25–30] the authors have

TABLE 1 Scheme of the three successive decomposition reactions of calcium oxalate monohydrate

First mass loss – step I°	$CaC_2O_4{\cdot}H_2O_{(s)} \rightarrow CaC_2O_{4(s)} + H_2O_{(g)}$	R1
Second mass loss – step II°	$CaC_2O_{4(s)} \rightarrow CaCO_{3(s)} + CO_{(g)}$	R2
Third mass loss – step III°	$CaCO_{3(s)} \rightarrow CaO_{(s)} + CO_{2(g)}$	R3

chosen this material since it is conventionally selected as reference substance for thermal calibration. Therefore, it has been possible to compare and discuss the elaborations highlighted in the indicated items (1) and (2) against a large number of published results dealing with the thermal behavior of this compound. Focusing on proposals of item (1), it is well known that the thermal decomposition of COM, which occurs under an inert atmosphere following the three successive decomposition steps (Table 1), has been widely investigated in view of determining the values of E, preexponential factor, and kinetic model exponent. In these studies, this is achieved by elaborating the TA information carried out, in particular, under constant heating rate constraint.[25,31–34] Some of these works exploit the TA and MS techniques to identify the reaction mechanisms involved in the indicated steps.[35–38] As alternative approach, in this work, the E is determined, for each of the three reaction steps, by elaborating the MS signals through consolidated kinetic models as those of Kissinger, Ozawa, and Starink. In addition, the MS signals have been further processed to calculate this parameter through suitable isoconversional procedures involving the known models of Friedman and Starink. Regarding item (2), as the main novelty, this study makes evident the fundamental role of the MS analysis in providing a correct interpretation of the chemical events occurring, in particular, during the II° step. Through a detailed analysis of the MS signals, it is possible to identify unambiguously the contemporary presence of the exothermic reaction of dismutation of CO into CO_2 and C-graphite. The relevance of this investigation lies in the fact that the presence of this reaction cannot be inferred by the elaboration of the mass loss measurements but only through a specific analysis of the MS signals. This enables to identify and quantify the volatile compounds CO and CO_2 evolving during this step, and, consequently, the contribution of the thermal effects of the indicated reaction within the global thermal balance of this II° event. These outcomes agree with the conclusions pointed out in an in-depth analysis of the thermal behavior of the COM recently published.[34]

2 | SAMPLE PREPARATION AND CHARACTERIZATION

2.1 | Chemical reagents and sample synthesis

Sodium oxalate (RS-grade, cod. 482101, CAS 62-76-0) and calcium chloride anhydrous (RS-grade, cod. 433535, CAS 10043-52-4) were purchased from Carlo Erba Reagents and used as received. Fresh bi-distilled water was used, stored in a plastic wash-bottle open to air atmosphere.

Calcium oxalate powder was prepared to exploit the different salt's solubility and avoiding acid–base reaction, following the precipitation reaction at room temperature by using the minimum water volume: $Na_2C_2O_{4(aq)} + CaCl_{2(aq)} \rightarrow CaC_2O_{4(s)} + 2\,NaCl_{(aq)}$.

4.585 g of pure sodium oxalate (34.2 mmol) was slowly dissolved by adding the minimum volume of distilled water (200 mL) under stirring at room temperature. Analogously, a second solution was easily prepared by dissolving 3.798 g of anhydrous calcium chloride (34.2 mmol) into 20 mL of distilled water. Then the $CaCl_2$ solution was added dropwise to the NaC_2O_4 solution under vigorous stirring. Immediately, a white precipitate was formed, the suspension was aged at room temperature for some hours, and, after stopping the stirring, the precipitate was left to spontaneously settle for several hours. The overlying transparent liquid phase, presenting a pH 6.8, was carefully removed by suction, while the remaining wet solid fraction was washed by adding 50 mL of distilled water. The resulting suspension was stirred for 15 min and left again to settle. The washing process was repeated three times. After the calcium oxalate powder was settled, the pH of each overlying washing was measured, finding the constant value of pH 6.8 (i.e., the value of the distilled water, used for washing). The suspension was then carefully filtered on a filter paper (retention grade $< 2\,\mu$m); the powder was dried in an oven at 80°C for 12 h and stored in a closed vessel. Finally, 4.728 g of powder was recovered (i.e., 32.3 mmol of $CaC_2O_4{\cdot}H_2O$; yield of 94.6%).

2.2 | Sample characterization

2.2.1 | Infrared spectroscopy analysis

The Fourier-transform infrared spectroscopy (FTIR) spectra of the obtained dried powder were recorded on a Varian Excalibur 4100 spectrophotometer working in ATR (attenuated total reflection) mode in the 4000–550 cm^{-1} range. The pure sample powder was laid on the diamond

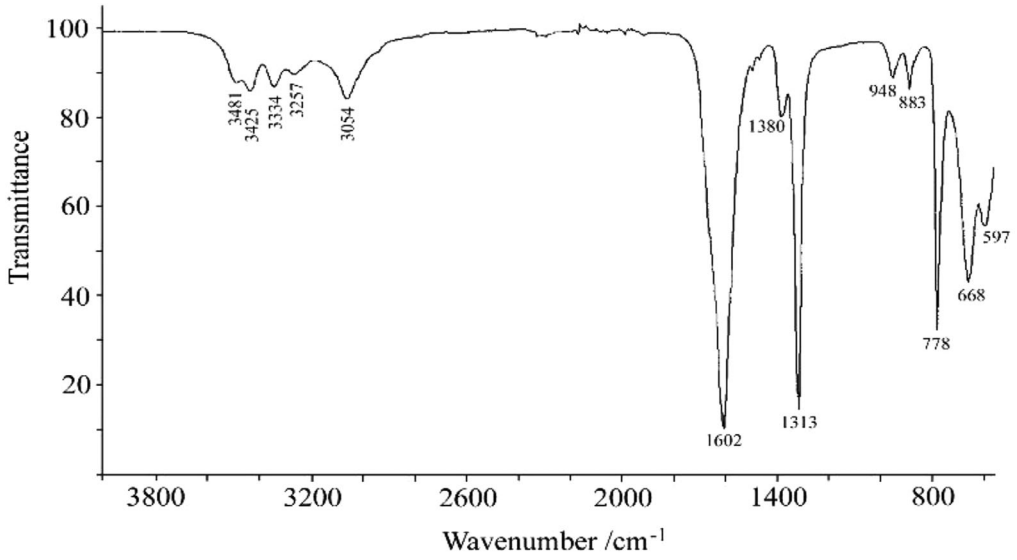

FIGURE 1 FTIR-ATR spectrum of the obtained calcium oxalate monohydrate

crystal (Golden Gate Specac Graseby) collecting 64 scans with a 4 cm^{-1} resolution. The ATR spectrum is reported in Figure 1.

2.2.2 | X-ray diffraction analysis

The crystal structure of the synthesized powder has been investigated through the x-ray diffraction (XRD) analysis carried out by an IPD3000 diffractometer equipped with a Co anode source (line focus) and a multilayer monochromator to suppress $k\beta$ radiation. The sample was measured in reflection geometry with a fixed incident angle of 5°. Diffraction data were collected by means of an Inel CPS120 detector over 5–120° 2θ range, 0.03° per channel, and an acquisition time of 60 min. The diffraction spectrum is reported in Figure 2.

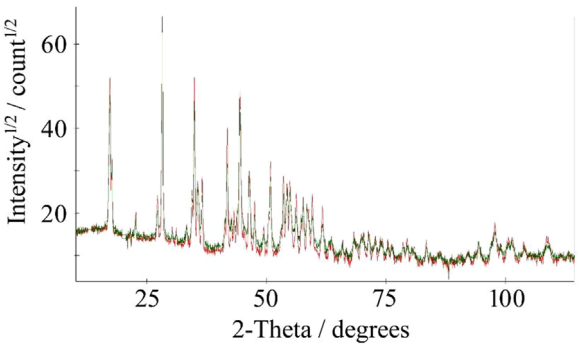

FIGURE 2 XRD pattern of the synthesized calcium oxalate monohydrate (green line). Comparison with the pure $CaC_2O_4{\cdot}H_2O$, COM, standard reagent (Sigma-Aldrich, cod C0350000, CAS 5794-28-5) (red line)

2.3 | Sample results

2.3.1 | FTIR characterization data

The FTIR-ATR spectrum of the synthesized powder, reported in Figure 1, shows a frequency pattern that well corresponds to the pure calcium oxalate monohydrate form: $CaC_2O_4{\cdot}H_2O$, COM. In particular, the presence of one single water molecule in the calcium oxalate solid structure gives rise, at room temperature, to the formation of the typical frequencies pattern in the 3500–2800 cm^{-1} range. As indicated in the work of Conti et al.,[39] the four fundamental O–H stretchings are detected at 3481, 3425, 3334, and 3054 cm^{-1}. On the other hand, the less intense fifth band at 3257 cm^{-1} could be assigned to the first overtone of the H–O–H bending, which fundamentally (at ca. 1628 cm^{-1}) could be lost in the overlap with the more intense band of the C=O stretching, justifying its asymmetric form.

So that, following the frequencies labeling described in Conti et al.,[40] the C=O stretching vibration, ν_{11}, originates the intense band at 1602 cm^{-1} while the second stretching ν_9 is revealed by the sharp peak at 1313 cm^{-1}. The less intense sharp peak at 778 cm^{-1} could be attributed to the in-plane OCO group bending ν_{12}, whereas the OCO out-of-phase rocking ν_{10} is detected by the small band at 1380 cm^{-1}. Finally, in this lower frequency region, the weak bands detected at 948 and 885 cm^{-1} are assigned to the vibrations of the water molecule in the COM solid structure.

2.3.2 | XRD characterization data

The XRD spectrum shows that the only crystal structure present in our synthesized powder samples is the calcium oxalate whewellite being its experimental diffraction pattern coincident with the whewellite ideal crystal structure COD (Crystallography Open Database) entry 9000763.[40–42] The calculation was made by the Rietveld program MAUD.[43] In particular, Figure 2 shows the pattern of our prepared sample (green line), in comparison with the one recorded for the pure standard-reagent counterpart, $CaC_2O_4{\cdot}H_2O$ (Sigma-Aldrich, cod C0350000, CAS 5794-28-5) (red line).

3 | INSTRUMENTATION AND EXPERIMENTAL PROCEDURES

3.1 | Thermal analysis

TGA and DTA were performed on a LabSys Setaram thermobalance, operating in the range 20–1000°C. Measurements were carried out fluxing the thermobalance furnace with He (99.999% purity) at a constant flow of 120 $cm^3{\cdot}min^{-1}$ (measured at 20°C and 0.1 MPa). Thermal analyses were recorded using similar amounts of powder (5.5–5.9 mg) and carried out by selecting, progressively, the following constant heating rates (β): 7, 10, 13, 16, 19, 22, and 25°C·min^{-1}. The sample powders were quickly weighed and loaded into alumina crucibles (volume 0.1 cm^3) then the thermobalance was immediately closed and purged with He flux adjusted and controlled by means of a Matheson mass flow controller. The thermobalance, previously kept under constant He flux and precharged with a standard amount of α-Al_2O_3 (8.7 mg) as reference compound, was quickly opened to insert the crucible sample and immediately closed. During this preliminary procedure, the He flux was increased up to 300 $cm^3{\cdot}min^{-1}$ by adding a supplementary flow from a second inlet port located at the bottom of the balance body. This condition has been maintained for ca. 30 min to promote the rapid removal of air from the apparatus, which achieves the inert atmosphere in a few minutes as proved by the exponential decay of the N_2 and O_2 IC signals detected by the mass spectrometer. The He was then restored to the operative (120 $cm^3{\cdot}min^{-1}$) flux to start the analysis.

3.2 | Mass spectrometry analysis

Mass spectrometric analysis was carried out using a TRIO-1 VG quadrupole mass spectrometer detector. The furnace of the thermobalance was connected with the ionization chamber of the mass spectrometer through a home-built transfer line[19] made with an empty and deactivated-silica capillary-column (0.32 mm internal diameter, 13.5 m length) enveloped in a thermostatic jacket heated at 238 ± 1°C. (This column length is required for maintaining the vacuum inside the mass spectrometer). During the thermal analyses, an appropriate fraction of the purging He flux sampled a few millimeters above the sample crucible, was continuously withdrawn and analyzed. Electron impact mass spectra (70 eV) were continuously recorded in the scan mode in the 1–400 amu range with the frequency of 1 scan s^{-1} (ionization chamber temperature 180°C). The quadrupole mass spectrometer was calibrated weekly by using perfluorotributylamine ($C_{12}F_{27}N$, CAS: 311-89-7) as reference, while operative parameters were tuned daily with particular attention to the improvement of the He signal. Operative experiments showed that gaseous species usually required less than 40 s to travel the whole transfer line before being detected. MS data are recorded as a continuous sequence of mass spectra so that any gas species released from the solid sample can be easily monitored by the detection of its fragmentation ion patterns in the recorded spectra. From these MS data, it is also possible to obtain both the total ion current curve (TIC graph) and the single contributions of any m/z ion current curve (IC graphs) versus time, that is, the linear increase of temperature recorded during the entire TA. The trend of the TIC curve reveals therefore the global release of the compounds, while each IC curve allows to monitor the presence of individual chemical species presenting appropriate m/z values belonging to particular ions not present in the fragmentation ion pattern of the other released compounds. In our experience, we usually observed that in TG-MS analyses repeated on the same sample under the same operative conditions when the temperature peaks differ for values minor of 1°. For this reason, the temperature values will be reported in the text without their decimal points.

4 | KINETICS MODELING

The use of dynamic TA represents a recognized experimental tool to study the kinetics of complex processes as those occurring during the thermal decomposition of solids. As well known, the obtained experimental results can be elaborated to set up a variety of kinetic models, the majority of which lead to the degradation rate to two functions: the $k(T)$ term to account for the temperature dependency and the $f(\alpha)$ function, depending only on the extent of conversion α, to express the reaction model scheme:

$$\frac{d\alpha}{dt} = k(T) \cdot f(\alpha). \quad (1)$$

The parameter α is conventionally defined as

$$\alpha = \frac{m_0 - m_{t,T}}{m_0 - m_\infty}, \tag{2}$$

where m_0 and m_∞ are the initial and the final mass of the sample, respectively, while the term $m_{t,T}$ indicates the mass of the sample referred to time t and temperature T. The $k(T)$ function can be successfully modeled by assuming the Arrhenius equation form:

$$k(T) = A \cdot \exp\left(-\frac{E}{RT}\right), \tag{3}$$

where A is the preexponential factor, E the apparent activation energy, and R the universal gas constant. Combining Equation (3) with Equation (1), the basic form of the kinetic equation is achieved:

$$\frac{d\alpha}{dt} = A \cdot \exp\left(-\frac{E}{RT}\right) \cdot f(\alpha). \tag{4}$$

In this study, all the runs of the TA have been carried out under constant heating constraint by selecting suitable values for the parameter $\beta = (dT/dt) = \text{const}$. By including it into Equation (4), the following differential form of the kinetic equation is derived:

$$\frac{d\alpha}{dT} = \frac{A}{\beta} \cdot \exp\left(-\frac{E}{RT}\right) \cdot f(\alpha). \tag{5}$$

The determination of the kinetic parameters of Equation (5) can be pursued following different approaches. Since the kinetic study proposed in this work limits only to E estimation, the so-called "model-free" methods have been adopted avoiding, therefore, the choice of suitable selections for the $f(\alpha)$ function. The models included in this work do not cover all the existing model-free methods but, from the knowledge of the authors, those considered here are widely utilized to describe the thermal degradation of solids. In the following subsections, a synthetic description of the selected models is proposed.

4.1 | Maximum reaction rate method

The method of Kissinger can be derived from Equation (5) when it is referred to the maximum reaction rate by imposing the constraint: $d^2\alpha/dt^2 = 0$. After simple elaboration,[44,45] the indicated equation can be rearranged to provide the conventional Kissinger equation form:

$$\ln\left(\frac{\beta}{T_m^2}\right) = \ln\left(-\frac{AR}{E_a} f'(\alpha_m)\right) - \frac{E}{RT_m}, \tag{6}$$

where the term $f'(\alpha_m)$ represents the $f(\alpha)$ derivative evaluated at the maximum reaction rate (α_m). The E can be determined from the slope of the straight line resulting from the plot of the left-hand side of Equation (6)versus $1/T_m$. This procedure requires, for each β, the value of the temperature T_m detected in correspondence to the maximum conversion rate that, rigorously, corresponds to the temperature of the flex point of the TG profile curve inside a specific mass loss event here indicated as T_f (flex point temperature). Since, at this condition, the corresponding α_m value can vary significantly with β, this procedure cannot rigorously be classified as "isoconversional" even if, due to this misunderstanding, it is usually confused with the isoconversional Kissinger–Akahira–Sunose (KAS) model. As evidenced in Starink's paper,[46] this condition can be approximated as a specific stage of the thermal reaction referred to as the maximum transformation rate (or reaction rate). Since the peak temperature points T_p of both the DTG and DTA profiles are achieved in correspondence to this condition, they can as well be utilized as substitutes of T_m in Equation (6). For sake of clearness, a representation of the T_f and T_p points, here introduced, is shown in Figure 5. Moving from this observation, two further equations, presenting a similar structure of Equation (6), have been considered in this work:

the first is the Ozawa equation[47,48]:

$$\ln(\beta) = \text{Const.} - 1.052\frac{E}{RT_m} \tag{7}$$

the second is the Starink equation[46]:

$$\ln\left(\frac{\beta}{T_m^{1,92}}\right) = \text{Const.} - 1.0008\frac{E}{RT_m}. \tag{8}$$

From Equations (7) and (8), the E can be as well determined following the procedure indicated for Equation (6). In this work, this approach has been extended by substituting the T_f (flex point temperature of the TG profile) or, alternatively, the T_p values (peak point temperature of the DTG or DTA profiles) for T_m. This procedure, requiring only the knowledge of these remarkable points, is here indicated as the maximum reaction rate (MRR) method.

4.2 | Isoconversional methods

As reported in reference papers including also the recommendations indicated by the Kinetics Committee of the International Confederation for Thermal Analysis and Calorimetry (ICTAC),[45,49] to which reference is made for

the fundamentals of these methods, the isoconversional principle states that the reaction rate at the constant extent of conversion is only a function of temperature. To obtain experimentally the temperature dependence of the isoconversional rate, a series of runs have to be performed. In this work, seven constant heating rates (β values) were chosen as indicated in Section 3.1. Two computational schemes can be elaborated to exploit the experimental results to derive the kinetic parameters of the studied processes: differential and integral methods. The most consolidated models representative of the differential methods are those of Friedman[50,51] and Flynn and Wall[52] expressed by Equations (9) and (10), respectively:

$$\ln\left(\beta \cdot \frac{d\alpha}{dT}\right) = \ln A + \ln f(\alpha) - \frac{E}{RT} \tag{9}$$

$$\ln(\beta) = \ln\left[A \cdot \frac{f(\alpha)}{d\alpha/dT}\right] - \frac{E}{RT} \tag{10}$$

The integral methods can be derived from the following generalized equation representative of the so-called "direct isoconversional methods":

$$\ln\left(\frac{\beta}{T^n}\right) = +\omega \cdot \frac{E}{RT} + \text{const} \tag{11}$$

By assigning the value $n = 0$ and $\omega = -1{,}052$ to the parameters, Equation (11) turns to the Ozawa equation (previous Equation (7)) known, in this contest, as the Flynn–Wall–Ozawa (FWO) isoconversional method, while, assigning to the parameters the values $n = 1{,}92$ and $\omega = -1{,}0008$, the Starink equation indicated in Equation (8) is obtained. When utilized within the isoconversional procedure it turns to the Starink isoconversional method. Assigning the values $n = 2$ and $\omega = 1$ to the coefficients, Equation (11) represents the KAS model already introduced in the previous section.

4.3 | Modeling procedure involving the MS analysis

4.3.1 | MS applied to the MRR method

As described in Section 4.1, distinctive remarkable points of the TA analysis can be applied to the MRR procedure to determine the E. Analogously, the peak temperature of the TIC curve ($T_{p,TIC}$) and the peak temperatures of the three representative IC curves ($T_{p,IC}$) corresponding to the released of H_2O, CO, and CO_2 molecules (at m/z 18, 28, and 44 u.m.a.) can be likewise exploited as input parameter for T_m in the same Equations (6)–(8). This represents a novel alternative option to determine the E by exploiting specific remarkable points of the evolution of the MS profiles within the same equations conventionally used for TA signals elaborations.

4.3.2 | MS applied to the isoconversional procedure

This section presents the procedure identified in this work to determine the E by applying the results of the MS signals to the isoconversional approach. Since the mass spectrometer apparatus utilized for the experimental campaign does not allow to export of the recorded data, the elaboration of the data has been limited by the operative procedures implemented in the instrument software. In particular, the procedure to determine the temperatures for each of the selected isoconversion points ($T_{\alpha=\alpha}$) for the three IC signals (m/z 18, 28, and 44) has required a complex sequence of elaborations here described. It must be pointed out that this operative program allows to directly calculate the area value below a band of an IC only when the initial and final points are chosen before and after the maximum of the obtained curve. For each released species (H_2O, CO, and CO_2), the area value (A) below the whole band of each IC molecular ion curve (A_{tot}) was measured in order to quantify its total released amount during that specific thermogravimetric event. Then the progressive nominal values of the areas corresponding to the conversion degrees from $\alpha = 0.1$ to $\alpha = 0.9$ were calculated ($A_{(\alpha=\alpha)\text{nominal}}$). Taking into account all these nominal values in correspondence to each chemical species, for each conversion degree value ($\alpha = \alpha$) and each heating rates, the integrations of the IC band were made, starting from the same constant initial point (initial time "$t_{initial}$") to a final one (t_j) in order to get an area value ($A_{(\alpha=\alpha)tj}$) more close to the nominal value of the selected area ($A_{(\alpha=\alpha)\text{nominal}}$). For example, for sake of clarity these steps are summarized in Figure 3 where in part (A) the shift on the temperature scale of the IC m/z 28 band is reported by increasing β while, in part (B), this procedure referred to $\alpha = 0.7$ is outlined. After the determination of an appropriate number (n) of these experimental points (usually n from 3–7), a graph of the area values versus their respective final time values is plotted. These points have been interpolated with a second-degree polynomial function to determine the nominal time value for the selected conversion degree value, $t_{\alpha=\alpha}$, as shown in Figure 4A. Then the t_α value has been converted to the corresponding temperature value $T_{\alpha=\alpha}$ by considering the respective heating rate β. Finally, for each released species and all the conversion degree values, the set of the $T_{\alpha=\alpha}$ temperature values was used to plot the "Arrhenius graph" by using the three KAS, FWO, and Starink($T^{1.92}$) equations

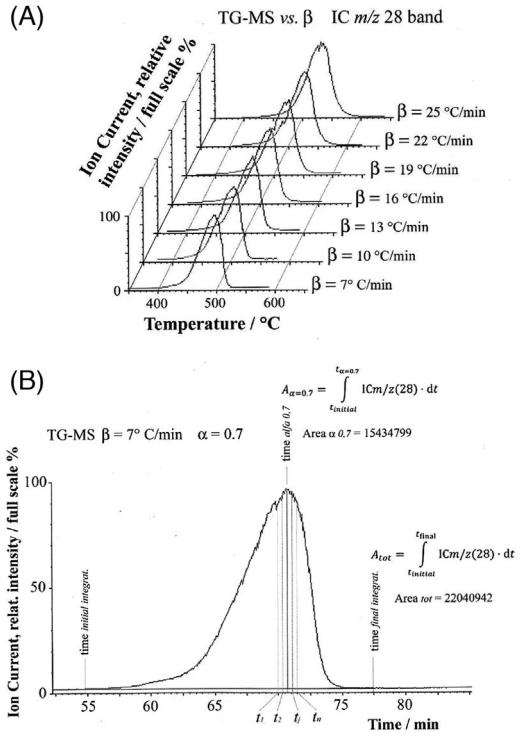

FIGURE 3 IC curve of the TG-MS analyses recorded at different β values for the isoconversion time data identification. (A) shift of the temperature with β for the IC m/z 28 band; (B) representation of the isoconversional procedure referred to $\alpha = 0.7$

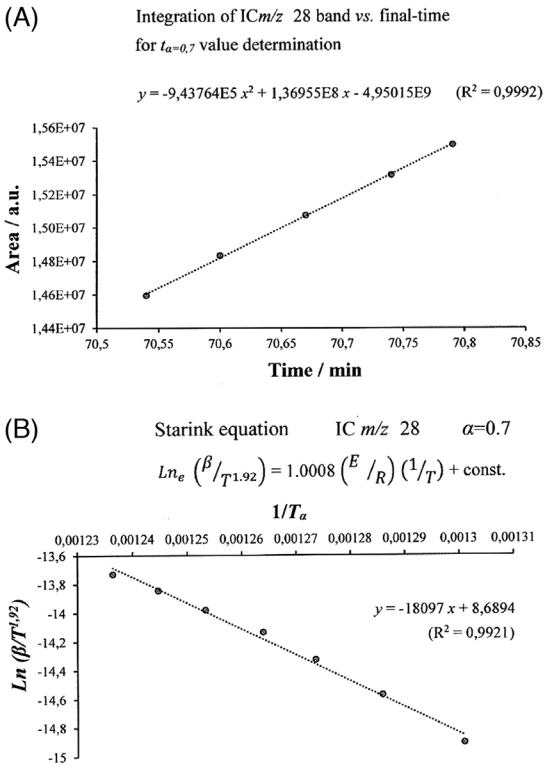

FIGURE 4 TG-MS analysis for the isoconversion temperatures and E determination. (A) interpolated function to determine the nominal time value for the selected conversion degree at $\alpha = 0.7$; (B) "Arrhenius graph" representation resulting by the application of the Starink equation

as exemplified in Figure 4B for the case of the Starink equation.

5 | PRESENTATION AND DISCUSSION OF THE *E* DETERMINATION

5.1 | Experimental results

Keeping in mind the parameters of the proposed MRR models, the thermal decomposition of COM has been characterized by identifying the remarkable points introduced in Sections 4.1 and 4.3.1: the flex temperature T_f of the TG-band curve, the peak temperature T_p of both the DTG and DTA-band curves, the peak temperature $T_{p,MS}$ of the TIC and the selected IC curves derived from the MS analysis. All these points have been detected for each of the three reactions reported in Table 1 and for each heating rate (β values). Figure 5 depicts the TG, DTG, and DTA curves and, in the upper part, the corresponding peak points ($T_{p,MS}$) of the TIC curve for the thermal run at $\beta = 7°C\ min^{-1}$.

Table 2 summarizes the experimental values of all the remarkable points for each of the selected β values. To simplify the presentation, the three reactions 1, 2, and 3 are indicated as Step I°, Step II°, and Step III°, respec-

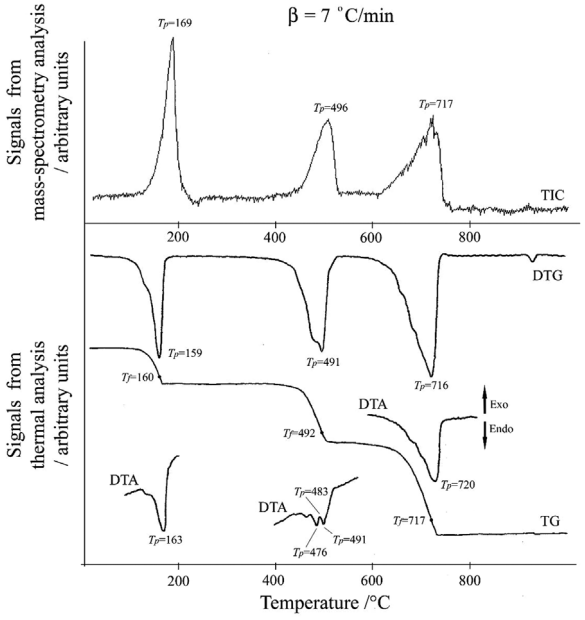

FIGURE 5 Thermal analysis (TG, DTG, DTA curves) and TG-MS analysis (TIC curve) for $\beta = 7°C \cdot min^{-1}$

TABLE 2 Flex temperature T_f of the TG-band curve, peak temperatures T_p of the DTG and DTA band curves, peak temperatures, $T_{p,TIC}$ and $T_{p,IC}$ from the TIC and IC curves of the MS analysis

TG, DTG, and DTA analysis									
	T_f of the TG curve (°C)			T_p of the DTG curve (°C)			T_p of the DTA curve (°C)		
β (°C·min^{-1})	Step I°	Step II°	Step III°	Step I°	Step II°	Step III°	Step I°	Step II°	Step III°
7	160	492	717	159	491	716	163	483	720
10	168	497	732	165	496	730.	171	493	735
13	172	504	740	168	500	736	176	503	741
16	176	508	747	170	502	738	179	510	748
19	180	512	754	175	506	747	185	515	758
21	182	515	757	176	508	748	186	518	762
25	186	518	765	179	511	752	189	522	768

MS analysis						
	$T_{p,TIC}$ of the TIC curve from MS (°C)			$T_{p,IC}$ of the IC curve from MS (°C)		
β (°C·min^{-1})	Step I°	Step II°	Step III°	m/z 18	m/z 28	m/z 44
7	169	496	717	170	499	724
10	179	505	737	179	508	737
13	187	512	746	187	515	751
16	196	518	754	198	520	762
19	212	523	761	213	525	770
21	218	528	770	219	529	776
25	233	533	774	233	533	783

tively. The table, in correspondence to the MS section, includes the peak temperatures ($T_{p,TIC}$) of the TIC curve and those of the IC curve ($T_{p,IC}$) corresponding to the m/z 18, 28, 44 signals for the species H_2O, CO, and CO_2, respectively. These peak points are utilized to replace T_m in Equations (6)–(8).

To better detail the results of the MS investigations, Figure 6 depicts, for all the selected β, the profiles of the IC curves within the temperature range of interest and highlights the peak temperature $T_{p,IC}$ whose values are included in Table 2. Figure 6 has been expressly included to highlight the shift of the $T_{p,IC}$ values as β increases.

To complete the overall view of the experimental section, the results of the temperature of the isoconversion points ($T_{\alpha=\alpha}$) in correspondence to the selected α value (α range: 0.1–0.9, step 0.1), for the three IC signals (m/z 18, 28, and 44) and each β, are included in Table 3. For sake of clearness, these values are obtained following the procedure described in Section 4.3.2.

5.2 | Models results

5.2.1 | MRR model

Figure 7 provides an overall overview of the E trends obtained from the application of the MRR models. For summary issues, the numerical values comprehensive of the uncertainties are summarized in Table A of the Supporting Information (SI). Figure 7 is split into three plots each one for the three equation models: Kissinger (A), Ozawa (B), and Starink (C). Furthermore, within each plot, the data are subdivided into the three mass loss events, relative to the course of reactions (1), (2), and (3), and where each dataset (histogram bar) are associated by a selected color (blue, green, red, respectively). Starting from the left side, the plots indicate the E values obtained from the TA elaboration (TG, TDG, DTA) while, on the right side, those derived from the MS signals, TIC and IC, respectively. It is to remember that the IC figures identify the first mass loss for m/z 18 (H_2O release), the second for m/z 28 (CO release), and the third for m/z 44 (CO_2 release).

5.2.2 | Isoconversional models

Figure 8 shows the E results of the isoconversion models introduced in Section 4.3.2. (See Table B of the SI for the numerical values.) Due to the feature of these methods, the E trend is depicted versus the extent of conversion α in the range $0.1 < \alpha < 0.9$ and, henceforth, when referred to the isoconversional option E will be indicated as E_α. In Figure 8, the E_α results are represented in two plots: on the left side of plot (A) the results are obtained by applying the differential Friedman model to the TA (Equation 9), on the right side by applying the FWO model to the MS signals

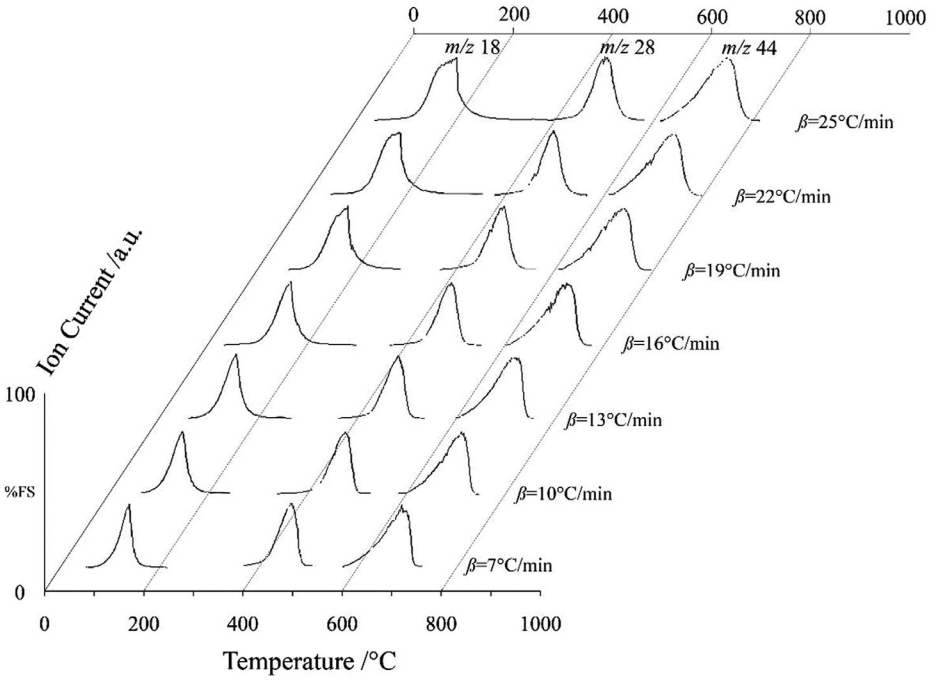

FIGURE 6 Trend of the molecular IC in correspondence to the release of H_2O, CO, and CO_2 species inside their, respectively, thermal event (I°, II°, and III°)

(Equation 11); plot (B depicts the E_α trends obtained by applying the isoconversional procedure only to the Starink equation (Equation 11) and specifically: the left side to TA, right side to the MS signals. Both plots (A) and (B) include also the average values for each reaction. Analogously to shown in Figure 7, the data arising from the three thermal events are represented with different colors.

5.3 | Discussion

5.3.1 | MRR models

A general overview shows that the E results are the same independently from the adopted MRR method (Figure 7). The Ozawa model provides results slightly higher if compared with those of Kissinger and Starink, practically equal within the uncertainty of the experimental error bands (see SI, Table A). Narrowing the view to the TA (Figure 7), the results of the DTG elaboration are always the highest for the three thermogravimetric events while those of the I° and III° events are quite similar both for the TG and the DTA analysis.

Looking specifically at the II° event, the E derived from DTA is always significantly lower compared to that from TG and DTG. This achievement is almost independent of the models as can be seen by calculating the ΔE % $[100\cdot(E_{\text{Tp-DTA}} - E_{\text{Tf-TG}})/E_{\text{Tf-TG}}]$ quantity that, selecting the TG curve as reference, provides −33.11%, −31.31, and −33.05% for the Kissinger, Ozawa, and Starink models, respectively (data from SI, Table A). As it will be deeply discussed in Section 6, it is precisely this behavior that has suggested for the second step to hypothesize the occurring of a further parallel reaction in addition to conventional reaction 2. Regarding the impact of the different signals, Figure 7 evidences that the E obtained from the MS are usually lower than those derived from the TA without significant differences from the adopted models.

Considering the results of the Starink model as case test and assuming the TG data as reference, the differences of the E calculated from the T_p of the TIC curve to the E derived from the T_f of the TG curve provides: −62.16%, −25.66%, and −16.69% moving from the I° to the III° step, respectively. This difference is particularly drastic for the dehydration of the calcium oxalate (I° step). Considering these discrepancies, one wonders about the reliability of these results that, ultimately, can be led back to the approximations adopted for the temperature integral. In the literature,[53] this condition is expressed in terms of the parameter $Y = E/RT$ whose variability must be verified and to be within $15 < Y < 60$. For the TIC and the IC analysis referred to the I° event (m/z 18), this constraint is never satisfied since the resulting values for the Y set, in any case, are below 10. When reference is made to the temperatures T_f of the TG curve or T_p of the DTA curve, the Y values are set around 20. Consequently, the E values of the dehydration step obtained from the MS analysis have to be considered unreliable while, for the II° and III°

TABLE 3 Experimental temperature $T_{(\alpha=\alpha)}$ for the three species: H_2O, CO, and CO_2 determined for each α values following the isoconversional procedure introduced in Section 4.3.2

IC (m/z)	Conversion (degree)	Temperature $T_{(\alpha=\alpha)}$ (°C) of the isoconversional TG-MS analysis						
		$\beta = 7$	$\beta = 10$	$\beta = 13$	$\beta = 16$	$\beta = 19$	$\beta = 22$	$\beta = 25$
18	$\alpha = 0.1$	131	141	147	149	161	165	169
18	$\alpha = 0.2$	144	153	160	165	174	179	184
18	$\alpha = 0.3$	152	161	168	174	183	188	195
18	$\alpha = 0.4$	158	167	174	180	191	196	203
18	$\alpha = 0.5$	162	172	180	186	198	203	212
18	$\alpha = 0.6$	166	177	185	192	204	209	219
18	$\alpha = 0.7$	170	1811	189	197	211	216	227
18	$\alpha = 0.8$	174	188	196	205	219	224	235
18	$\alpha = 0.9$	188	204	213	225	245	246	262
28	$\alpha = 0.1$	458	461	471	476	480	485	492
28	$\alpha = 0.2$	468	474	483	488	493	500	505
28	$\alpha = 0.3$	476	482	491	497	501	508	513
28	$\alpha = 0.4$	482	489	497	503	508	515	519
28	$\alpha = 0.5$	487	494	502	508	514	521	525
28	$\alpha = 0.6$	491	500	507	513	520	526	530
28	$\alpha = 0.7$	495	504	512	518	525	530	536
28	$\alpha = 0.8$	500	509	517	523	530	535	541
28	$\alpha = 0.9$	505	515	522	528	536	543	549
44	$\alpha = 0.1$	652	671	679	682	692	695	702
44	$\alpha = 0.2$	665	688	696	700	711	714	721
44	$\alpha = 0.3$	676	700	709	713	724	728	735
44	$\alpha = 0.4$	686	710	719	725	735	739	746
44	$\alpha = 0.5$	693	718	727	734	744	749	755
44	$\alpha = 0.6$	700	726	735	741	752	757	764
44	$\alpha = 0.7$	706	732	742	749	761	765	773
44	$\alpha = 0.8$	712	739	748	756	768	773	781
44	$\alpha = 0.9$	718	746	755	763	776	781	789

events, since the Y set in the range $20 \leq Y \leq 46$, they look acceptable.

5.3.2 | Isoconversional models

Comparing the performances of the isoconversional methods applied to TA and reported in the left sides of plots A and B of Figure 8, the differential model of Friedman and the integral model of Starink present a similar trend. For the three events and all over the α range the Starink model provides lower values. With reduced differences, similar trends can be observed for the FWO and Starink models (right side of plot A and plot B, respectively) obtained from the MS signals elaborations. The correspondent numerical values of these plots are reported in Table B of the SI. Regarding the reliability of these results, the constraints of the Y parameter introduced in the previous section are in this case as well satisfied with the exception of the E_α results of the I° event obtained from the TIC and IC elaborations. This confirms, therefore, the criticalities pointed out for the MRR models. Looking at the sequence of the events and at the impact of the two signals (TG and MS), the results of the MS signals are always lower than those derived from the TA with a decreasing trend moving from the I° to the III° events. For the I° event (dehydration), the E_α decreases as α increases. This is in accordance with the results of recent study[42] dealing with the characterization of the crystal structure of the calcium oxalate. This study demonstrates that the progressive release of water entails a progressive modification of the interactions of the residual water molecules with the solid structure that, consequently, affects the E_α evolution as dehydration occurs. From the point of view of the authors, the cited study is considered particularly relevant since the sample powder preparation has followed a very close procedures adopted

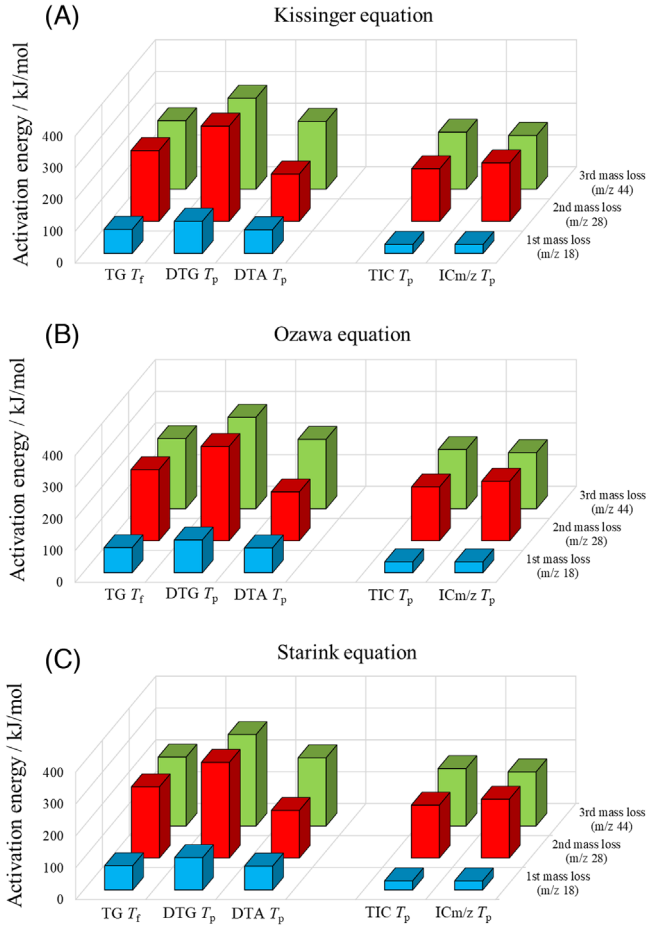

FIGURE 7 *E* trend results of the MRR method of Kissinger (A), Ozawa (B), and Starink (C) applied to TA and MS analysis for the three decomposition reactions (blue color for the first, red color for the second, and green color for the third mass loss)

for the investigation here proposed. These factors, probably, play a more limited role in the release of CO and CO_2 molecules involved in the II° and III° events. To this concern, it must be noted that in reaction 2 and 3 the energy demand to break the covalent chemical bonds inside the oxalate and carbonate molecular structure accounts for a higher contribution to form and release the CO and CO_2 species with respect to that required to break the only physical interaction required for the water molecule release from the solid crystal network; all that in agreement with the *E* values of the first event which are at least halved or less compared to those of the II° and III° event.

For the II° event, the plots evidence that the E_α value referred to TG signal and for $\alpha = 0.1$ (Figure 8, left side) is significantly smaller than the others. Only in correspondence to the central α range, the E_α reaches roughly constant values as can be observed for the trends derived from the MS signal with the exception of the extreme cases, $\alpha = 0.1$ and 0.9 in Figure 8 (right side). From the point of view of the authors, these discrepancies are probably due to a higher error in calculating the relative area values from the partial integration of the IC signal (see Section 4.3.2).

As final observation, the E_α trends obtained from the TG analysis (Figure 8, left side) present a significant scattering, while those referred to the MS signals (Figure 8, right side) present a reduced background noise so that, the use of MS signals, allows to obtain for E_α a better defined trend.

5.4 | Comparison with literature data

The reliability of the obtained *E* results has been tested versus literature sources. Despite the relevant number of studies dedicated to COM decomposition, the comparison is proposed with respect to the outcomes reported in Anderson et al.'s paper.[54] This publication ranks significantly since the reported results have been obtained by the kinetic working group of the German Society of Thermal Analysis by processing 144 experimental TG datasets conforming to the Round Robin Test protocol.

The results of the investigations carried out in our work, subdivided for each reaction, have been compared with those of the cited work[54] gathered, for each step, within their ranges with the *E* values expressed in kJ $kmol^{-1}$:

- *First event*[54]: $78.4 \leq E \leq 104.35$. These values are consistent with the results of Tables 6 and 7 of the SI. Excluding the problems evidenced for the MS analysis referred to the first step, the *E* values set within the lower value: $E = 74.9$ (Kissinger) (not too far from the lower indicated limit) and the higher $E = 103.5$ (Ozawa, DTG). Similarly, the average value of the isoconversional method sets at $E_\alpha = 91.2$ and $E_\alpha = 83.8$ for Friedman and Starink, respectively.
- *Second step*[54]: $213.6 \leq E \leq 261.56$. The results of the MRR methods, obtained from the TG signals, are set within this range for the three selected models (Kissinger, Ozawa, Starink; see Table A in the SI). For all the other models, including the isoconversional methods, the achieved *E* values are lower than those reported in the cited publication. The *E* values derived from the DTA signals are set below the lower limit while those from the DTG are set above the upper. This behavior will be better analyzed in Section 6.
- *Third step*[54]: $192.9 \leq E \leq 225.9$. The results of the MRR method, referred to as the TG and the DTA signals, set within the indicated range for the three examined models. Furthermore, they are above the indicated upper limit (225.9) for the DTG signal elaborations (see Table A in SI). The values derived from the three models applied to the MS signals are close to the lower indicated limit. This can be seen in particular for the TIC signal

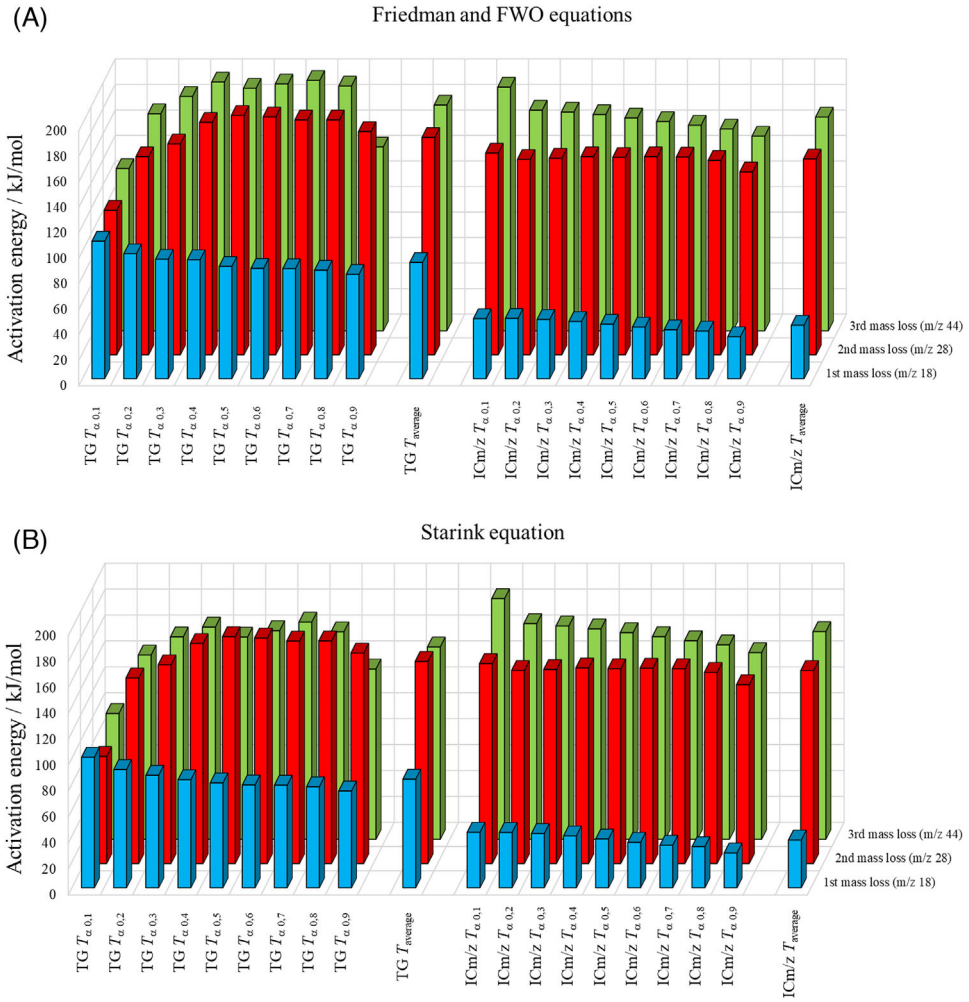

FIGURE 8 (A) E_α isoconversion results of the Friedman model (left-side) from TA and the FWO model (right side) from MS; (B) isoconversional procedure applied to the Starink model from TA (left-side) and MS (right side). Blue color for the first, red color for the second, and green color for the third mass loss

TABLE 4 Peak temperature $T_{p(ICm/z44\text{-}II°event)}$ of the IC m/z 44 band signals in correspondence of the II° event for the selected heating rates

MS analysis	
B (°C·min^{-1})	$T_{p(ICm/z44\text{-}II°event)}$ (°C)
7	496
10	506
13	513
16	519
19	526
22	529
25	533

including the error band ranges (Table 4, second section). This trend is also confirmed for the isoconversional models limiting the results to $0.3 \leq \alpha \leq 0.8$ in particular for the Friedman model. (See Table B in SI.)

6 | INVESTIGATION OF THE SECONDARY REACTION IN THE SECOND THERMAL STEP

6.1 | Experimental results

In all the TG-MS analysis recorded at the selected β the trend of the IC m/z 44 ion current (used to monitor the CO_2 evolution) presents the formation of a smaller band in the range 365–600°C in correspondence to the oxalate decarbonylation reaction (second event), besides the CO_2 development occurring during the carbonate decomposition (third event in the temperature range: 600–850°C). Indeed, the mass spectra recorded inside this small band disclose, although with a modest intensity, the presence of the m/z 44 ion confirming the presence of CO_2. These events are shown in Figure 9, which includes also the mass spectra detected at the T_p of the two bands for the analysis carried out at $\beta = 25$°C/min for example.

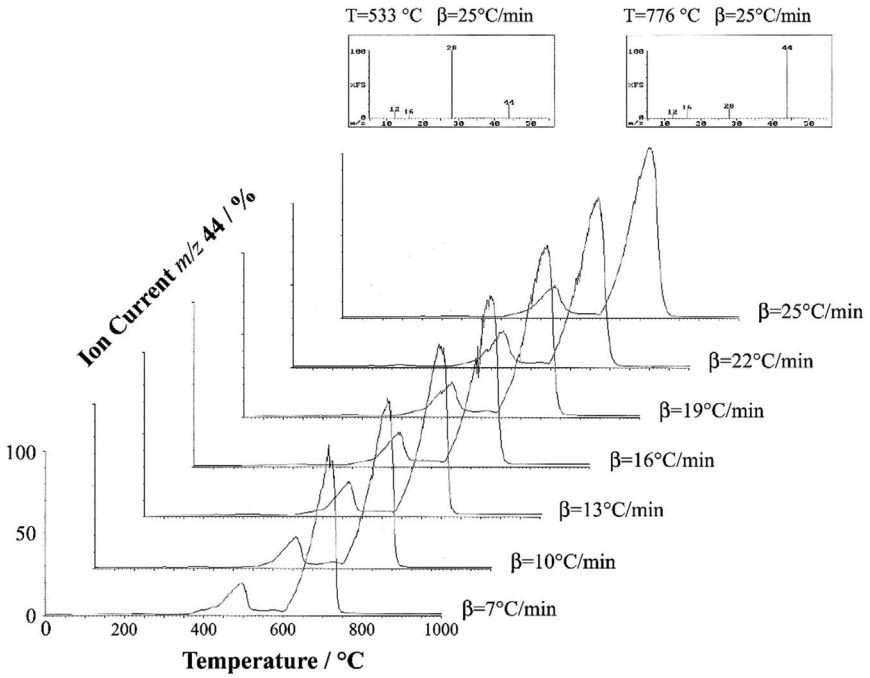

FIGURE 9 IC m/z 44 trends to monitor CO_2 evolution during the second and third thermal events. In the insets, the mass spectra recorded at the T_p of the two bands in the $\beta = 25°C \cdot min^{-1}$ TG-MS analysis

The peak temperatures of these IC m/z 44 smaller bands inside the second thermal event, $T_{p(ICm/z44\text{-}II°event)}$, are reported in Table 4.

6.2 | Modeling

The detection of CO_2 during the thermal decomposition of calcium oxalate unequivocally indicates the occurrence of a further secondary reaction during the second step. To the authors knowledge, this CO_2 formation, mentioned in some papers[30,34,55,56] is always led back to a partial (or total) oxidation of CO, yielded from reaction 2, following the stoichiometry:

$$CO + 1/2 \cdot O_2 \rightarrow CO_2$$

even though the thermal process is claimed to be carried out under an inert atmosphere neglecting, therefore, any justification pertaining to the oxygen source. The presence of CO_2 is also supported by the exothermic effect measured from the DTA or DSC signals during this decomposition process.

Considering the following observations emerging during our TG-MS experiments campaign:

- the powder recovered at the end of the entire TG-MS analysis (or when the measure is arbitrary stopped after the II° event) presents a gray color instead of white as expected for the formation of pure calcium oxide (or calcium carbonate);
- the different and irregular shape of the DTA profile observed for the II° event with respect to those pertaining to the I° and III° steps (Figure 5), where the contribution of a more modest exothermic band seems to overlap on the original development of the expected endothermic band of reaction 2;
- the different (lower) mass-loss percentage-value of this II° event that always we detected with respect to the nominal one associated with pure oxalate into carbonate decomposition.

This makes it right to consider the thermal dismutation of CO into CO_2 and carbon graphite as a second consecutive reaction. This reaction, occurring during the II° step (also known as the Boudouard reaction), take places in the gas-phase and leads to the CO_2 formation without requiring an oxidizing counterpart:

$$\text{secondary reaction–step II } 2 \cdot CO_{(g)} = CO_{2(g)} + C_{(s)} \quad \text{(R4)}$$

Moreover, at these temperatures, the yielded carbon graphite immediately sublimated to the solid-state covering both the residual solid sample, the sample holder, and the internal chamber of the thermobalance modifying, therefore, the measured mass-loss of this second event.

The E of this reaction has been determined by applying the Kissinger, Ozawa, and Starink MRR method (see Section 5.2.1) to the peak temperatures ($T_{p(ICm/z44\text{-}II°event)}$)

TABLE 5 *E* values of the CO dismutation reaction obtained from the IC *m/z* 44 signals by applying the MRR method to the Kissinger, Ozawa, and Starink equations

***E* of the dismutation reaction**				
Equation	***E* (kJ mol^{-1})**	**Uncertainty**	**R^2**	***Y***
Kissinger	163.3	3.0	0.9983	24.8
Ozawa	167.7	2.8	0.9986	25.5
Starink	163.7	3.0	0.9983	29.4

TABLE 6 Summative equation scheme of the II° event

(Quantitative course, $\alpha = 1$)	$CaC_2O_{4(s)} \rightarrow CaCO_{3(s)} + CO_{(g)}$	R2
(Partial course, $\alpha = \alpha$)	$CO_{(g)} \rightarrow ½\ C_{(s)} + ½\ CO_{2(g)}$	R5
(II° global thermal event)	$CaC_2O_{4(s)} \rightarrow CaCO_{3(s)} + (1\text{-}\alpha)\ CO_{(g)} + (\alpha/2)\ C_{(s)} + (\alpha/2)\ CO_{2(g)}$	R6

reported in Table 4. The results are summarized in Table 5 together with the values of the uncertainty, the R^2, and the *Y* parameter introduced in Section 5.3.1.

Figure 10 depicts the "Arrhenius graph" as a result of the data-processing procedure applied to the Starink equation. It is important to highlight that it has been possible to determine the *E* of this secondary reaction only by monitoring the IC *m/z* 44 signal within this second event where only the CO should be the expected species.

6.3 | Discussion

In order to study the effective course of the CO dismutation reaction, the relative percentage of the CO_2 yielded during the entire course of the II° thermogravimetric event has been estimated. Figure 11 presents for $\beta = 7$°C/min, the trends of the TIC profile and those of the IC curves of the H_2O, CO e CO_2 species including the area of each of the detected IC bands that are proportional to the amount of the species released during the thermal event. In the insets above the curves, the mass spectra recorded at the T_p of the TIC bands are also included. During the I° and III° event, the mass spectra highlight, as expected, the exclusive presence of H_2O and CO_2 while, during the II° event, the recorded mass spectra show, besides the expected CO yielded from reaction 2, the minor presence of CO_2 yielded from the partial occurrence of the CO dismutation reaction.

Considering the areas of the two bands referred to the IC *m/z* 44 and 28 curves of the II° and III° event, an amount of 4.3 mol% of CO_2 has been calculated as specific contribution of the II° event (details of this elaboration are reported in Section A of SI). Considering the equations scheme of Table 6, this event can be entirely described as the sum of the quantitative course of reaction 2 by adding reaction 4 which does not occur quantitatively (in this scheme included as reaction 5 with a ½ stoichiometry), leading to the indicated global reaction 6.

Considering the presence of the CO_2 in the evolved gas-phase ($_{mol}\%(CO_2) = 4.3$), a stoichiometric elaboration allows to quantify the course of reaction 5 ($\alpha_{R5} = \alpha$) with respect to the quantitative course of the reaction 2($\alpha_{R2} = 1$), yielding the following conversion degree whose details are reported in Section B of the SI:

$$\alpha_{R5} = 2/(1 + 100/_{mol}\%(CO_2)) = 0.0825$$

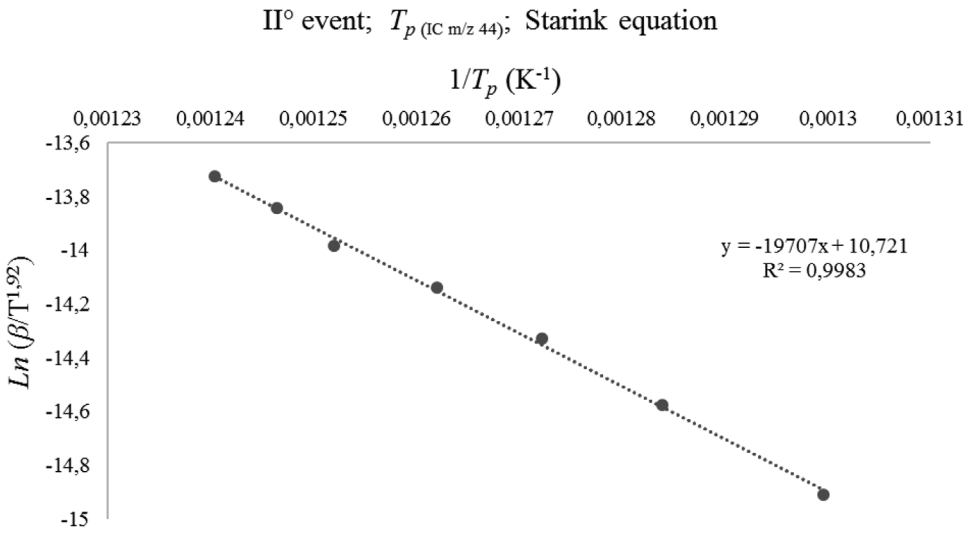

FIGURE 10 Arrhenius graph elaboration of the CO dismutation reaction obtained by applying the Starink MRR method to the $T_{p(ICm/z44\text{-}II°event)}$ values

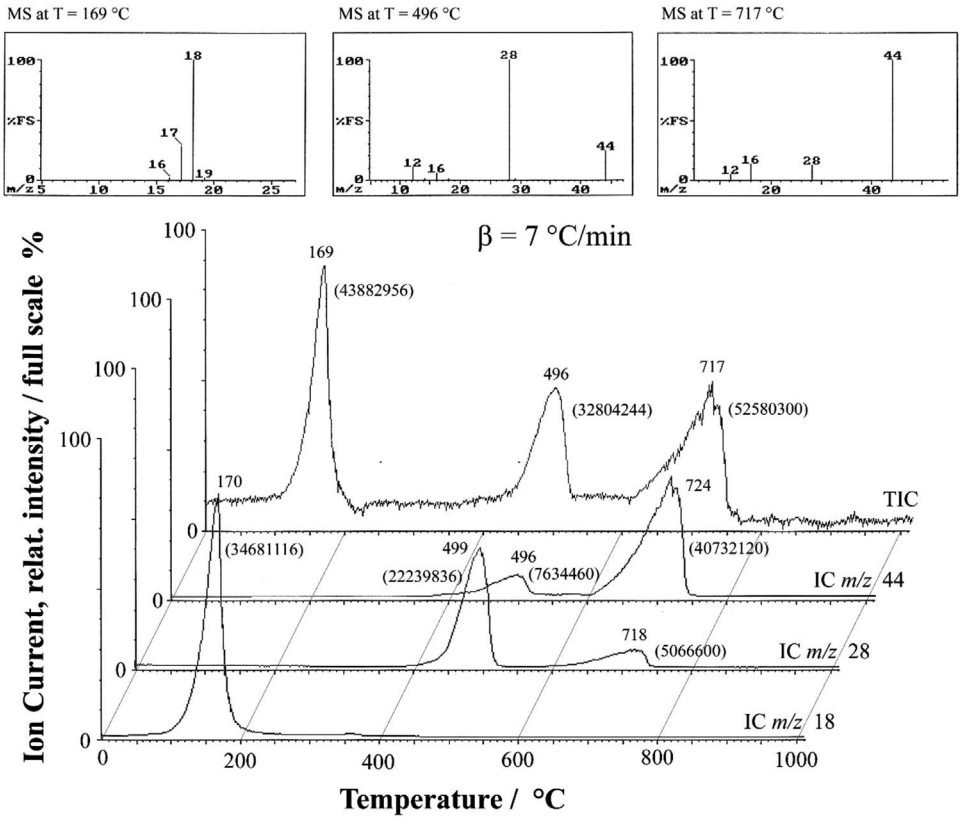

FIGURE 11 TG-MS analysis carried out at $\beta = 7°C \cdot min^{-1}$. TIC and IC curves of the released H_2O, CO, and CO_2 species. In the inset, mass spectra recorded at the T_p of the TIC curve

The standard enthalpy of reaction 4, $\Delta H°_{R4}$, at 496°C has been carefully calculated by considering the enthalpy data of the involved species available in the literature.[57,58] Unlikely, the standard enthalpy of reaction 2 has been only roughly estimated since the temperature dependency of the specific molar heat (c_p) of calcium oxalate anhydrous and monohydrate was not found so that they have been kept constant at the reference temperature (25°C). Detailed elaborations are reported in Section C of the SI.

With this assumption the standard enthalpy of reactions 2 and 4 becomes, respectively:

$$\Delta H°_{R2} = 43.212 \text{ and } \Delta H°_{R4} = -178.728 \text{ kJ/mol}$$

while for reaction 5 trivially halves: $\Delta H°_{R5} = -89.364$.

The total enthalpy of the II° event, reaction 6, becomes, therefore

$$\Delta H°_{R6} = \Delta H°_{R2} + \Delta H°_{R5} \cdot \alpha_{R5} = +35.839 \text{ kJ/mol}$$

Moreover, it must be noted that the spontaneity course of reaction 4 course is confirmed by the negative value of the standard free energy of the reaction: $\Delta G°_{R4} = -35.99$ kJ/mol (calculated at 496°C).

In conclusion, during this II° thermal event a percentage decrease of the global enthalpy effect, due to the partial course of the CO dismutation reaction, can be quantified:

$$\Delta(\Delta H°)\% = 100 \cdot (\Delta H°_{(react.6)} - \Delta H°_{(react.2)})/\Delta H°_{(react.2)} = -17.1\%$$

Surprisingly this result is very close to the percentage decrease observed for the E calculated, with the MRR method, from the T_p of the IC m/z 28 bands and the T_f points of the TG curves through the Starink equation:

$$\Delta(E)\% = 100 \cdot \left(E_{Tp-ICm/z28} - E_{Tf-TG}\right)/E_{Tf-TG} = -17.3\%$$

In this regard, it is to remember that the two signals provide the following information:

- The latter (TG-curve) is unable to detect the course of reaction 4 since it only monitors the effects of the mass variation due to the oxalate decomposition into the carbonate in a quantitative transformation ($\alpha_{R2} = 1$);
- the former (IC m/z 28) is able to specifically detect the effective presence of the CO species; therefore, the effect

of reaction 2 (which quantify its production) together with those of reaction 4 (which quantifies its partial course) provides the real global course of this II° event occurring in the gas phase.

Concerning the E, a second remarkable correlation can be found among the values resulting from the MS analysis. The first pertains to the E obtained by processing the T_p of the II°-TIC-bands whose signal monitors all the events occurring in this temperature range (i.e., the course of reaction 6). The second concerns the E referred to the course of each one of the single reactions 2 and 4 (characterized by opposite endo-exo-thermally effects) obtained by evaluating the T_p of the bands of the IC m/z 28 and 44 signals detected inside the II° thermal event.

When these two last E values are weighted with the molar percentage of the corresponding CO and CO_2 species evolved in the gas phase, the weighted E value results very close to that obtained from the TIC curve.

In fact, in the hypothesis of considering that the endo-exo-thermally effects of these two reactions act in contrast with each other and also taking into account the uncertainty of these E values, obtained from the Starink equations, the so obtained values can be considered almost coincident:

$$
\begin{aligned}
E_{\mathrm{II^\circ TIC-band}} &= 166.0 \pm 3.4\ \mathrm{kJ/mol} \\
E_{\mathrm{average}} &= E_{(\mathrm{R2})\cdot \mathrm{mol}}\%(\mathrm{CO}) - E_{(\mathrm{R4})\cdot \mathrm{mol}}\%(\mathrm{CO_2}) \\
&= E_{(\mathrm{Tp-IC28-II^\circ event})\cdot \mathrm{mol}}\%(\mathrm{CO}) \\
&\quad - E_{(\mathrm{Tp-IC44-II^\circ event})\cdot \mathrm{mol}}\%(\mathrm{CO_2}) \\
&= [(184.7 \pm 1.5) \cdot 0.957] \\
&\quad - [(163.7 \pm 3.0) \cdot 0.043] \\
&= 169.7 \pm 1.6\ \mathrm{kJ/mol}
\end{aligned}
$$

This fact confirms general feedback often observed in our experimental TG-MS measurements. In the course of a complex endothermic thermal decomposition event, characterized by the contemporaneous occurrence of different chemical reactions, the apparent activation energy value obtained elaborating the TIC signal results equal to that obtained from the average of the E values calculated for each of the single reaction and weighted by the molar composition of the corresponding product of these reactions.[59,60] This obviously occurs only if the complex decomposition event is previously correctly described by the complete identification of all the involved reactions pattern.

7 | CONCLUSIONS

The E involved in the three steps decomposition of calcium oxalate monohydrate has been determined by adopting both the MRR and the isoconversional procedures. An innovative approach has been proposed by coupling the conventional TA with MS signals elaborations.

Examining the results of the MRR method, the E trends are practically independent of the adopted models (Kissinger, Ozawa, Starink). Referring to the elaborated signals (TG, DTG, DTA, TIC, and IC for m/z 18, 28, and 44), the higher values of E are achieved indifferently from the TG and DTA signals elaborations while, for the II° reaction, the E calculated from the DTA signals is significantly lower than those derived from the TG elaborations. This discrepancy, thoroughly investigated by exploiting the potentiality of the coupled TG-MS technique, has allowed us to identify the occurrence of the CO dismutation (Boudouard reaction). The extended elaborations of the MS signals to the isoconversional methods have evidenced that the E_α trends are independent of the adopted equation models (Friedman, FWO, and Starink). Within the limits of these preliminary outcomes, the MS signals approach introduced in this study looks promising as reliable alternative for the E calculation. The consistency of the achieved results has been checked by the consolidated criterion expressed in terms of the parameter $Y = E/RT$. Some questions are still open as the unreliable E values obtained for the I° reaction and derived from the IC and TIC signals elaborations. Nevertheless, this study extensively confirms most of the results available in the literature. The proposed approaches look particularly suitable to encourage the application of the TG-MS techniques to the kinetic analysis.

DATA AVAILABILITY STATEMENT

Data are available on request from the authors.

ORCID

Maurizio Grigiante https://orcid.org/0000-0001-8115-2847

REFERENCES

1. Vyazovkin S, Wight CA. Isothermal and non-isothermal kinetics of thermally stimulated reactions of solids. *Int Rev Phys Chem*. 1998;17:407–433.
2. Prins MJ, Ptasinski KJ, Jassen FJJG. Torrefaction of wood. Part 1. Weight loss kinetics. *J Anal Appl Pyrolysis*. 2006;77:28–34.
3. Starink MJ. Activation energy determination for linear heating experiments: deviations due to neglecting the low temperature end of the temperature integral. *J Mater Sci*. 2007;42:483–489.

4. Wang J, Zhao H. Pyrolysis kinetics of perfusion tubes under non-isothermal and isothermal conditions. *Energy Convers Manage*. 2015;106:1046-1056.
5. Chen C, Ma X, He Y. Co-pyrolysis characteristics of microalgae *Chlorella vulgaris* and coal through TGA. *Bioresour Technol*. 2012;117:264-273.
6. Jeong H, Seo M, Jeong S, et al. Pyrolysis kinetics of coking coal mixed with biomass under non-isothermal and isothermal conditions. *Bioresour Tecnnol*. 2014;155:442-445.
7. Ferrara F, Orsini A, Plaisant A, Pettinau A. Pyrolysis of coal, biomass and their blends: performance assessment by thermogravimetric analysis. *Bioresour Technol*. 171:433-441.
8. Sonoyama N, Hayashi J. Characterisation of coal and biomass based on kinetic parameter distributions for pyrolysis. *Fuel*. 2013;114:206-215.
9. Zhang J, Chen T, Wu J, Wu J. TG-MS analysis and kinetic study for thermal decomposition of six representative components of municipal solid waste under steam atmosphere. *Waste Manage*. 2015;43:152-161.
10. Niu Z, Liu G, Yin H, Wu D, Zhou C. Investigation of mechanism and kinetics of non-isothermal low temperature pyrolysis of perhydrous bituminous coal by in-situ FITR. *Fuel*. 2016;172:1-10.
11. Seo DK, Park SS, Kim YT, Hwang J, Yu T. Study of coal pyrolysis by thermogravimetric analysis (TGA) and concentration measurements of the evolved species. *J Anal Appl Pyrolysis*. 2011;92:209-216.
12. Scaccia S. TG-FTIR and kinetics of devolatilization of Sulcis coal. *J Anal Pyrolysis*. 2013;104:95-102.
13. Ding L, Zhou Z, Guo Q, Lin S, Yu G. Gas evolution characteristics during pyrolysis and catalytic pyrolysis of coals by TG-MS and in a high-frequency furnace. *Fuel*. 2015;154:222-232.
14. Nowicki L, Ledakowicz S. Comprehensive characterization of thermal decomposition of sewage sludge by TG-MS. *J Anal Appl Pyrolysis*. 2014;110:220-228.
15. Han F, Meng A, Li Q, Zhang Y. Thermal decomposition and evolved gas analysis (TG-MS) of lignite coals from southwest China. *J Energy Inst*. 2016;89:94-100.
16. Wang M, Li Z, Huang W, Yang J, Xue H. Coal pyrolysis characteristics by TG-MS and its late gas generation potential. *Fuel*. 2015;156:243-253.
17. Yu D, Chen M, Wei Y, Niu S, Xue F. An assessment on co-combustion characteristics of Chinese lignite and eucalyptus bark with TG-MS technique. *Powder Technol*. 2016;294:463-471.
18. Jayaraman K, Kok MV, Gokalp I. Thermogravimetric and mass spectrometric (TG-MS) analysis and kinetics of coal-biomass blends. *Renewable Energy*. 2017;101:293-300.
19. Campostrini R, D'Andrea G, Carturan G, Ceccato R, Sorarù G. Pyrolysis study of methyl-substituted Si-H containing gels as precursors for oxycarbide glasses by combined thermogravimetric, gas choromatographic and mass spectrometric analysis. *J Mater Chem*. 1996;4:585-594.
20. Di Maggio R, Campostrini R, Guella G. Gels from modified zirconium n-botoxide: a pyrolysis study by coupled thermogravimetry, gas chromatographic and mass spectrometric analyses. *Chem Mater*. 1998;10:3839-3847.
21. Melendi-Espina S, Alvarez R, Diez MA, Casal MD. Coal and plastic waste copyrolysis by thermal analysis-mass spectrometry. *Fuel Process Technol*. 2015;137:351-358.
22. Nelson PF, Smith IW, Tyler RJ, Mackie JC. Pyrolysis of coal at high temperatures. *Energy Fuel*. 1988;2:391-400.
23. Coe FL, Evan A, Worcester E. Kidney stone disease. *J Clin Invest*. 2005;115:15-20.
24. Scales CD Jr, Smith AC, Hanley JM, Saigal CS. Prevalence of kidney stones in the United States. *Eur Urol*. 2012;62:160-165.
25. Anderson HL, Kemmler A, Hohne GWH, Heldt K, Strey R. Round robin test on the kinetic evaluation of a complex solid state reaction from 13 European laboratories. Part 1. Kinetic TG-analysis. *Therm Acta*. 1999;332:33-53.
26. Gao Z, Amasaki I, Nakada M. A description of kinetics of thermal decomposition of calcium oxalate monohydrate by means of the accommodated Rn model. *Therm Acta*. 2002;25:95-103.
27. Vlaev L, Nedelchev N, Gyurova K, Zagorcheva M. A comparative study of non-isothermal kinetics of decomposition of calcium oxalate monohydrate. *J Anal Appl Pyrolysis*. 2008;81:252-262.
28. Sadovska G, Wolf G. Enthalpy of dissolution and thermal dehydration of calcium oxalate hydrates. *J Therm Anal Calorim*. 2015;119:2063-2068.
29. Honcova P, Svoboda R, Pilny P, et al. Kinetic study of dehydration of calcium oxalate trihydrate. *J Therm Anal Calorim*. 2016;124:151-158.
30. Hourlier D. Thermal decomposition of calcium oxalate: beyond appearances. *J Therm Anal Calorim*. 2019;136:2221-2229.
31. Masuda Y, Ito Y, Ito R, Iwata K. Kinetic study of the thermal dehydration of calcium oxalate monohydrate. *Thermochim Acta*. 1986;99:205-215.
32. Kutaish N, Aggarwal P, Dollimore D. Thermal analysis of calcium oxalate samples obtained by various preparative routes. *Thermochim Acta*. 1997;297:131-137.
33. Budrugeac P, Segal E. Non-isothermal kinetics of reactions whose activation energy depends on the degree of conversion. *Thermochim Acta*. 1995;260:75-85.
34. Svoboda R, Zmrhalova ZO, Galusek D, Brandova D, Chovanec J. Thermal decomposition of mixed calcium oxalate hydrates—kinetic deconvolution of complex heterogeneous processes. *Phys Chem Chem Phys*. 2020;22:8889-8901.
35. Kaloustian J, Pauli AM, Pieroni G, Portugal H. The use of thermal analysis in determination of some urinary calculi of calcium oxalate. *J Therm Anal Calorim*. 2002;70:59-973.
36. Kaloustian J, El-Moselhy TF, Portugal H. Determination of calcium oxalate (mono- and dihydrate) in mixtures with magnesium ammonium phosphate or uric acid: the use of simultaneous thermal analysis in urinary calculi. *Clin Chim Acta*. 2003;334:117-129.
37. McGhie AR. Simultaneous thermogravimetry-differential thermal analysis-mass spectrometry (TG-DTA-MS) using a heated capillary interface. *Thermochim Acta*. 1994;234:21-29.
38. Frost RL, Weier ML. Thermal treatment of whewellite: a thermal analysis and Raman spectroscopic study. *Thermochim Acta*. 2004;409:79-85.
39. Conti C, Casati M, Colombo C, Realini M, Brambilla L, Zerbi G. Phase transformation of calcium oxalate dihydrate-monohydrate: effects of relative humidity and new spectroscopic data. *Spectrochim Acta A*. 2014;128:413-419.
40. Conti C, Casati M, Colombo C, et al. Synthesis of calcium oxalate trihydrate: new data by vibrational spectroscopy and

synchrotron X-ray diffraction. *Spectrochim Acta A*. 2015;150:721-730.
41. Tazzoli V, Domeneghetti C. The crystal structures of whewellite and weddellite: re-examination and comparison. *Am Mineral*. 1980;65:327-334.
42. Izatulina AR, Gurzhiy VV, Krzhizhanovskaya M, Kuz'mina MA, Leoni M, Frank-Kamenetskaya OV. Hydrated calcium oxalates: crystal structures, thermal stability and phase evolution. *Cryst Growth Des*. 2018;18:5465−5478.
43. Gražulis L, Lutterotti L. Total pattern fitting for the combined size-strain-stress-texture determination in thin film diffraction. *Nuclear Inst Methods Phys Res B*. 2010;268:334−340.
44. Kissinger HE. Reaction kinetics in differential thermal analysis. *Anal Chem*. 1957;29:1702−1706.
45. Vyazovkin S, Burnham AK, Criado JM, Pérez-Maqueda LA, Popescu C, Sbirrazzuoli N. ICTAC Kinetics Committee recommendations for performing kinetic computations on thermal analysis data. *Thermochim Acta*. 2011;520:1−19.
46. Starink MJ. The determination of activation energy from linear heating rate experiments: a comparison of the accuracy of isoconversion methods. *Thermochim Acta*. 2003;404:163−76.
47. Ozawa T. A new method for analysing thermogravimetric data. *Bull Chem Soc Japan*. 1965;38:1881-1886.
48. Ozawa T. Kinetic analysis of derivative curves in thermal analysis. *J Therm Anal*. 1970;2:301-324.
49. Brown ME, Maciejewski M, Vyazovkin S, et al. Computational aspects of kinetic analysis. Part A: the ICTAC kinetics project: data, methods and results. *Thermochim Acta*. 2000;355:125-143.
50. Friedman HL. Kinetics of thermal degradation of char-forming plastics from thermogravimetry. Application to a phenolic plastic. *J Polym Sci, Part C: Polym Lett*. 1964;6:183-195.
51. Friedman HL. New methods for evaluating kinetic parameters from thermal analysis data. *J Polym Sci Part B Polym Lett*. 1969;7(1):41-46.
52. Flynn JL, Wall LA. General Treatment of the Thermogravimetry of Polymers. *J Res Nat Bur Stand*. 1966;70A:487-493.
53. Starink MJ. A new method for the determination of activation energies for experiments performed at constant heating rate. *Thermochim Acta*. 1996;288:97-104.
54. Anderson HL, Kemmler A, Hohne GWH, Heldt K, Strey R. Round robin test on the kinetic evaluation of a complex solid state reaction from 13 European laboratories. Part 1. Kinetic TG-analysis. *Thermochim Acta*. 1999;332:33-53.
55. Gurrieri S, Siracusa G, Cali R. Thermal decomposition of CaC_2O_4 H_2O: determination of kinetic parameters by DTG and DTA. *J Therm Anal*. 1974;6:293-298.
56. Gadalla AMM. Kinetics of the decomposition of hydrated oxalates of calcium and magnesium in air. *Thermochim Acta*. 1984;74:255-272.
57. Barin I. *Thermochemical Data of Pure Substances*. 3rd edition. Weinheim Germany: VCH; 1995.
58. Weast RC, Astle MJ, Beyer WH. *CRC Handbook of Chemistry and Physics*. 68th ed. Boca Raton FL: CRC Press; 1987–1988.
59. Campostrini R, Sicurelli A, Ischia M, Carturan G. Pyrolysis study of a hydride-sol-gel silica Part 1. Chemical aspects. *J Therm Anal Calorim*. 2007;89:633-641.
60. Campostrini R, Sicurelli A, Ischia M, Carturan G. Pyrolysis study of a hydride-sol-gel silica Part 2. Kinetic aspects. *J Therm Anal Caoriml*. 2007;90:179-184.

SUPPORTING INFORMATION

Additional supporting information may be found online in the Supporting Information section at the end of the article.

How to cite this article: Campostrini R, Grigiante M, Brighenti M. Potentialities of mass spectrometry on activation energy and secondary reactions determination of calcium oxalate thermal decomposition. *Int J Chem Kinet*. 2021;53:1082–1100. https://doi.org/10.1002/kin.21504